INCEEUROPE

8th International Conference
on
Wind Turbine Noise
Lisbon Portugal – 12th to 14th June 2019

Experimental Investigation of Self-Aligning Trailing Edge Serrations for Airfoil Noise Reduction

K. Stahl, F. Manegar, Th. Carolus
University of Siegen, 57078 Siegen, Germany

R. Binois
Senvion GmbH, Überseering 10, 22297 Hamburg, Germany

Corresponding author: kathrin.stahl@uni-siegen.de

Summary

Turbulent boundary layer trailing edge noise is considered to be the dominant noise mechanism in wind turbines. An effective noise attenuation add-on is saw-tooth serrations attached to the trailing edge. The serration amplitude and the wavelength are the main geometrical variables. This experimental study investigates another geometrical variable, the so-called serration flap angle. Two different serrations were attached to a two-dimensional DU93W210 airfoil segment and tested in the Acoustic Wind-Tunnel (AWB) of the German Aerospace Center (DLR) in Braunschweig at a Reynolds number of 1.2 mio. The experiment was carried out in two steps. Firstly, different *fixed* flap angles had been tested in order to find the acoustically most efficient flap angle. Secondly, *self-alignment* of the serrations was allowed, while the airfoil angle of attack was varied.
The initial hypothesis that self-aligning serrations are superior when the airfoil angle of attack is varying (e.g. due to gusts of pitch control) can partly be confirmed. More noise reduction is possible with steeper than self-aligning flap angles of the serration, adapted to each airfoil angle of attack. Then the serrations need to be fixed. Fixed serrations as an add-onto a blade, however, result in an increase of the flow induced force on the blade just due to the net increase of blade area - the streamwise pressure distribution is not affected by the existence of serration.

Nomenclature

Symbols	Units	Description
c	m	chord length
c_p	-	pressure coefficient
f	Hz	frequency
$L_{p(1/3)}$	dB	sound pressure level (1/3- octave band)
LE	-	leading edge
PS	-	pressure side
Re	-	Reynolds number
Ref	-	reference (i.e. without serrations)
SS	-	suction side
TE	-	trailing edge
u_∞	m/s	velocity
α_{eff}	°	effective angle of attack
α_{geom}	°	geometric angle of attack
δ	mm	boundary layer thickness
ϕ	°	flap angle (fixed serrations)
ϕ_{sa}	°	flap angle (self-aligning serrations)
λ	m	width of serrations (wave length)

1. Introduction

For modern large horizontal axis wind turbines, aerodynamic noise from the blades is generally considered to be the dominant noise source, provided that mechanical noise is adequately treated [1]. The noise generated by the blade can be tonal or broadband in character, and may be caused by several mechanisms, such as the turbulent boundary layers across the trailing edge (TE) (subsequently denoted as trailing edge noise), laminar boundary layer vortex shedding, vortices from blunt trailing edges, or the induced secondary flow in the blade tip region [2]. Several studies consider trailing edge noise to be the dominant noise of a wind turbine [3]. Saw-tooth shaped serrations as an add-on at the trailing edge of a blade are a common noise reduction technique for TE noise mitigation. The acoustically “optimal” “tooth length (or amplitude)” and “width (or wave length)” relative to the local airfoil boundary layer thickness δ have been determined in a previous study. The flap angle ϕ, i.e. the angle between the streamwise direction of the serrations and the tangent to the profile, has been studied by ARCE in case of a NACA 0018 airfoil [4, 5]. It is felt, however, that more work is required concerning the effect of the flap angle. Furthermore, since add-ons like serrations in principle can increase the load on the blade, the effect of self-aligning flexible serrations is investigated. It is hypothesized that (i) self-aligning serrations are superior when the angle of attack to the blade is varying (e.g. due to

gusts of pitch control), (ii) self-aligning serrations produce a noise reduction without increase of blade load.

In this work two different serrations were attached to a two-dimensional DU93W210 airfoil segment. A wide range of different fixed flap angles were tested and assessed in a wind tunnel experiment. Eventually, also self-alignment of the serrations was allowed utilizing a hinge.

2. Airfoil Segment and Experimental Setup

Airfoil segment

Experimental investigations were carried out with a DU93W210 as the reference airfoil segment, equipped with serrations, Fig. 1. The model for the investigations in this paper has a chord length *c* of 0.3 m (*x*/*c* = 1 always indicates the trailing edge (TE) of the airfoil without serrations) and a span of 0.8 m. The DU93W210 is an airfoil with a maximum thickness of 0.21*c*, dedicated to wind turbine application and developed at the Delft University of Technology [6]. The thickness of the trailing edge of the airfoil (not the serrations) is 0.005*c* and hence 1.5 mm. Boundary layer tripping was applied close to the leading edge using a 0.2 mm zigzag trip on the suction side and 0.4 mm zigzag trip strip on the pressure side, Fig. 2. For measuring the chordwise pressure distribution on the pressure (PS) and suction side (SS) at mid-span 39 and 15 static pressure taps, respectively, are used. Naturally, close to the TE and along the serrations pressure taps were not feasible.

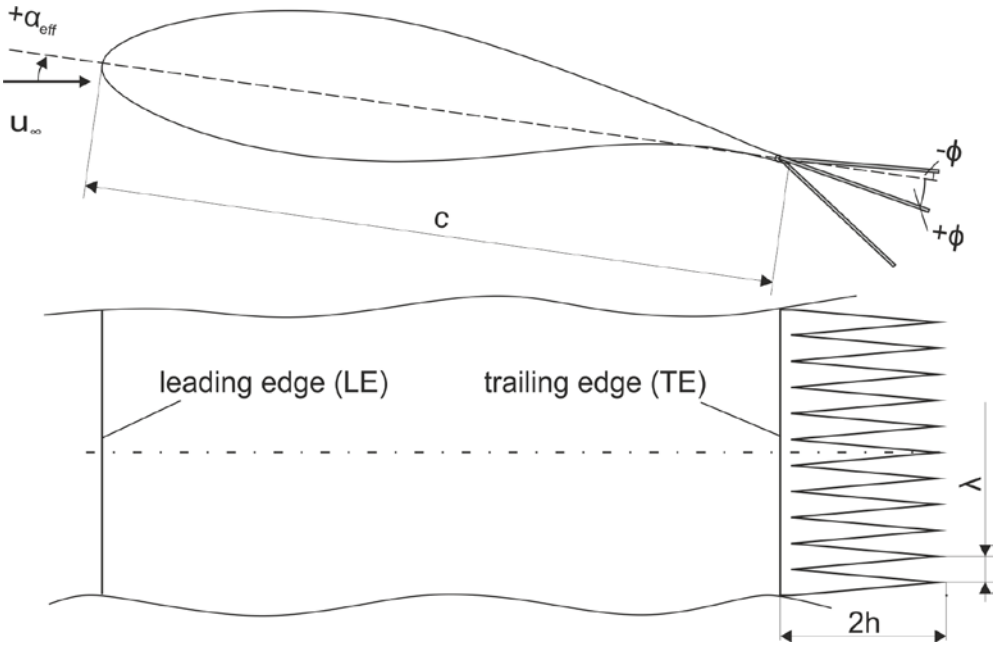

Figure 1: Airfoil and serrations.

The geometrical tooth and wave length of the serrations were selected according to a previous numerical Lattice-Boltzmann aeroacoustic simulation study.

Among eight different serrations with ratios of h/δ from 1.5 to 2.25[1] and λ/h from 0.2 to 0.6 the maximum efficiency in TE noise reduction was achieved for $h/\delta = 2$ and $\lambda/h = 0.35$.[2] Hence, these geometric dimensions are used for the trailing edge serrations named here S *I*. For practical reasons serrations S *II* with a somewhat shorter tooth as compiled in Tab. 1 and slightly less reduction capability were investigated as well.

Table 1: Geometry of serrations used in this study

	TE boundary layer thickness[1]	Absolute dimensions		Non-dimensional dimensions	
Denomination	δ [mm]	h [mm]	λ [mm]	h/δ [-]	λ/h [-]
S *I*	16	32	11.3	2	0.35
S *II*	16	24	7.5	1.5	0.31

All serrations were Laser cut from sheet metal of 0.5 mm thickness and attached to the TE via a hinge along the complete span. This allows self-aligning of the serrations in the flow, but various fixed flap angles could also realized with a set screw at the side plates. Fig. 3 shows the airfoil segment assembly ready for wind tunnel testing.

Figure 3: Airfoil assembly for experimental tests.

Experimental design

The experiments were carried out in two steps. Firstly, different *fixed* flap angles ranging from $\phi = -2.4°$ to $+33.6°$ in steps of 6° of the serrations *S I* were tested. Objective was to identify the acoustically most efficient flap angle. Throughout this test

[1] The boundary layer thickness $\delta = 16$ mm at the TE was derived from a XFOIL simulation for an effective angle of attack to the airfoil $\alpha_{eff} = 3.5°$ and a Reynolds number of 1.2 mio.

[2] Similar results can be seen by GRUBER et al. [7].

the airfoil angle of attack was set to α_{eff} = 3.5°. Secondly, *self-alignment* of the serrations was allowed using serrations type *S II*, while the airfoil angle of attack was varied from α_{eff} = 2.5° to 3.5° and 4.5°. In addition, as soon as the self-aligning flap angle ϕ_{sa} was determined, fixed flap angles of $\Delta\phi$ = ± 4° around each ϕ_{sa} were set. A summary of the parameter tested is given in Tab. 2. All measurements were done at a flow velocity of u_∞ = 60 m/s which corresponds to Re = 1.2 mio.

Table 2: Test parameters α_{eff} *and* ϕ for the parametric study, "*sa*" = self-aligning

Experiment	α_{eff}	Serrations	ϕ
Fixed flap angle study	3.5°	*S I*	0° (Ref), -2.4°, +3.6°, +9.6°, +15.6°, +21.6°, +27.6°, +33.6°
Self-aligning flap angle study	2.5°	*S II*	Ref, ϕ_{sa}, ϕ_{sa} + 4°, ϕ_{sa} - 4°
	3.5°		Ref, ϕ_{sa}, ϕ_{sa}+4°, ϕ_{sa} - 4°
	4.5°		Ref, ϕ_{sa}, ϕ_{sa} + 4°, ϕ_{sa} - 4°

Aero-acoustic wind tunnel

The experiment was carried out in the Acoustic Wind Tunnel Braunschweig (AWB) of the DLR. The AWB is an open-jet low noise facility with a rectangular nozzle exit of 0.8 m by 1.2 m and a maximum flow velocity of 65 m/s, as shown in Fig. 4. Sound absorbing linings at the chamber walls, floor and ceiling enable measurements at free field conditions for frequencies f > 250 Hz [8]. The dimensions of the anechoic chamber surrounding the free jet are 6.9 m x 6.9 m x 3.5 m with a test section length of 3.65 m [9]. The airfoil is mounted horizontally between two vertical side plates which are mounted to the nozzle. Integrated rotatable plates allowed the variation of the angle of attack.

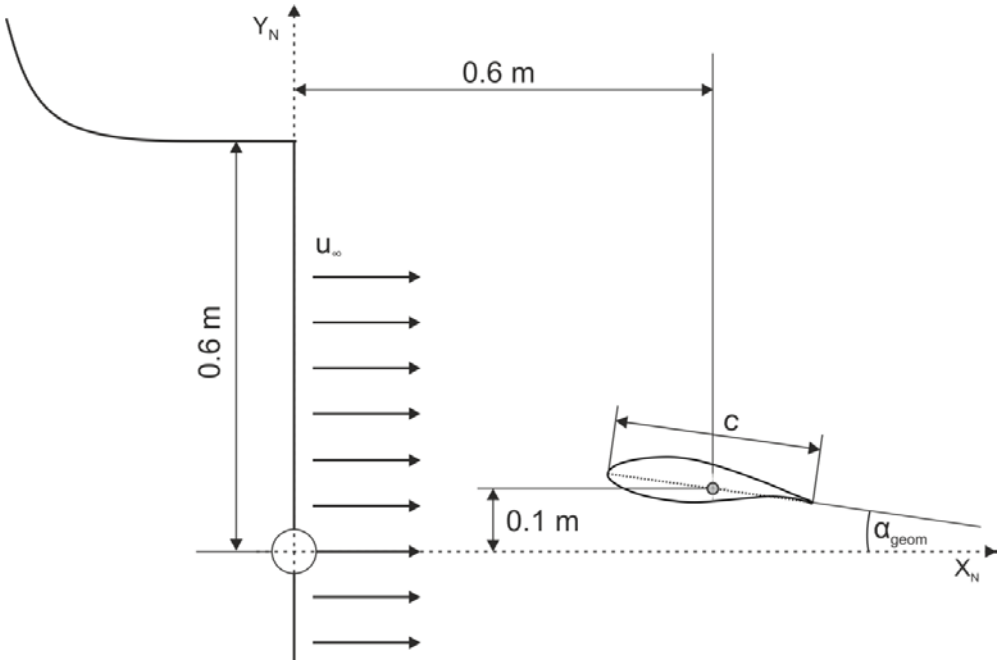

Figure 4: Experimental setup in the Acoustic Wind Tunnel Braunschweig (AWB).

Measurement techniques and data reduction

The static pressure distribution is obtained from the static pressure at each pressure taps in terms the pressure coefficients $c_p = (p-p_\infty)/0.5\rho u_\infty^2$. The measurements were made using a PSI 8400 acquisition system coupled with two 32 pressure ports scanner modules. The sampling rate was set to 50 Hz and averaged static pressure values were computed from 15 samples. The PSI 8400 system performs automatically the calibration and offset correction of the pressure modules [10].

Acoustic data were acquired through an elliptical mirror system pointing to the pressure side of the blade section and a microphone array (96 microphones pointing to the suction side) to determine noise radiated to either side, Fig. 5. Sound data were recorded at a sampling rate of 52 kHz. FFT signal processing resulted in a narrowband frequency bandwidth of Δf = 12.7 Hz. Other acquisition and processing parameters are: 16-bit dynamic range, 30 s measurement time, 30 kHz anti-aliasing low-pass filter, 500 Hz high-pass filter, Hanning window.

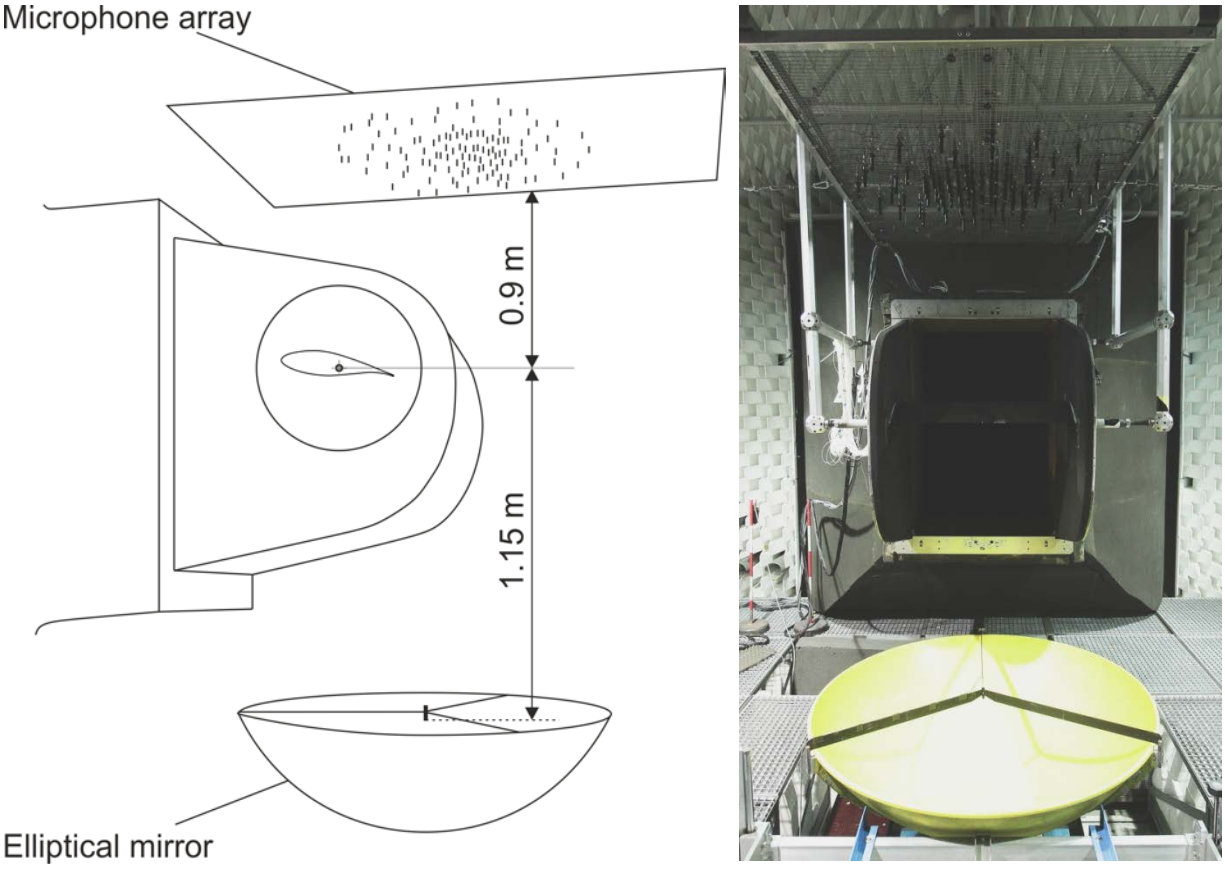

Figure 5: Measurement techniques in the experimental set up: Elliptical mirror and microphone array.

The mirror is mounted on a traverse. By moving the mirror in chordwise direction at mid-span below the airfoil section a localization of the noise source is possible. For all measurements mirror axis was oriented at 90° to the wind tunnel centre line. A calibrated 1/4-inch (6.35 mm) condenser microphone (Brüel & Kjær type 4136) was used. To provide absolute TE noise levels and to recover the “true” spectral shape,

extensive corrections of the directional microphone data where performed. These account for: (i) Sound wave convection, (ii) extraneous wind-tunnel noise sources, (iii) system response function (effective spatial resolution and gain) and (iv) source distribution. Shear-layer refraction and scattering effects are negligible for frequencies $f \leq 10$ kHz [11] and were not corrected. Nevertheless, the lowest frequency to be resolved is 1 kHz. All results are presented in one-third octave sound pressure levels ($L_{p(1/3)}$).The microphone array has an aperture of 0.97 m and is located at a distance of 0.9 m above the blade's SS in the TE region. Except for directivity effects these measurements are expected to provide redundant TE sound information when compared to the mirror measurement data. The determination of absolute TE noise levels from the phased array data is done using diagonal removal and the CLEAN-SC method [12]. The microphone array measurements allow for cross checking the mirror results while also indicating the source distribution on the complete segment.

Effective angle of attack

For an airfoil in a confined jet, it is essential to identify the effective angle of attack for each set geometrical angle of the segment in the wind tunnel. This is due to the fact that the lift produced in a confined jet is not the same as the finiteness of the jet leads to significant flow deflection. A comparison of a calculated pressure distribution with the pressure distribution from the wind tunnel establishes a relationship between the two angles as in Table 3. The pressure distribution is calculated employing XFOIL by DRELA [13]. (As in the experiment, a turbulent flow is also forced in the simulation. The tripping positions are at 0.02c on the suction side and at 0.05c on the discharge side, Fig. 6 shows the distributions.)

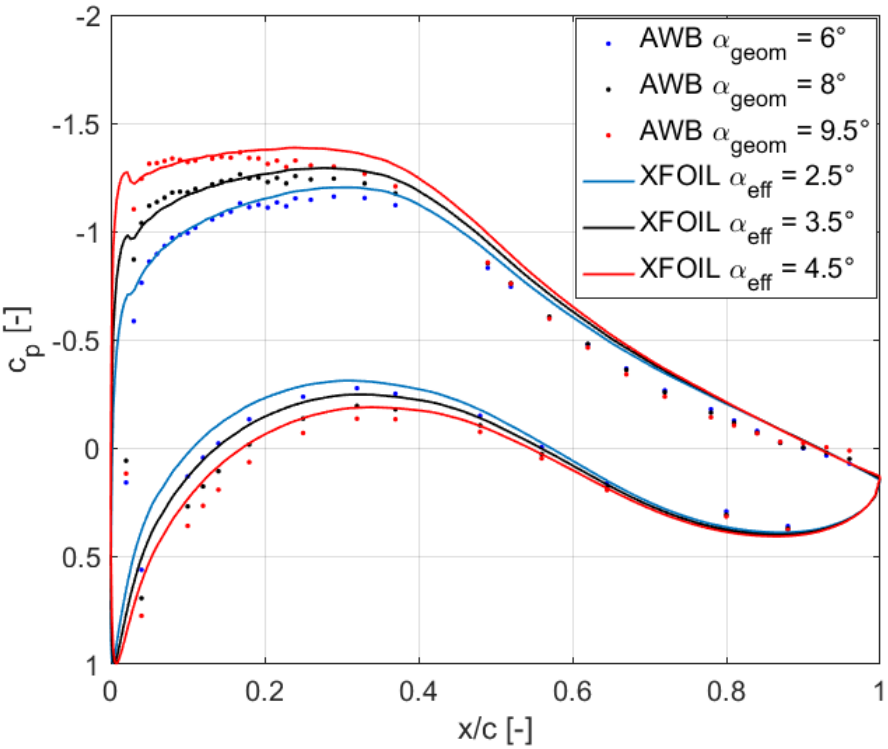

Figure 6: Measured and XFOIL-predicted static pressure distributions for corresponding geometrical and effective angles of attack.

Table 3: Corresponding geometrical and effective airfoil angles of attack

α_{geom}	6°	8°	9.5°
α_{eff}	2.5°	3.5°	4.5°

3. Results and Discussion

Fig. 7 depicts sound pressure maps for several 1/3-octave bands as obtained from the microphone array data. The reference airfoil and the airfoil with fixed flap angle (ϕ = 9.6°) at α_{eff} = 3.5° are compared. The effect of the serrations in the trailing edge region is clearly visible.

A more quantitative analysis is given in the next paragraphs. Fig. 8 shows the dependency of the spectra on ϕ for serrations S *I.* The four plots in Fig. 8 a) stem from the microphone array, in Fig. 8 b) from the mirror. In general, the results are independent of the measuring method. Since the signal-to-noise ratio is better with the mirror, only the mirror diagrams Fig. 8 a) are discussed further. A noise reduction can be observed irrespective of the flap angle up to the so-called cross-over frequency. The cross-over frequency is where serrations produce more sound than the airfoil without serration, here somewhere in the 1.6 or 2 kHz 1/3-octave band. As pointed out earlier, the lowest frequency resolvable by the mirror is 1 kHz. It is expected that the serrations are an effective mean for noise reduction far below this 1 kHz limit. As an example the noise reductions $\Delta L_{p,1/3}$ (i.e. sound pressure level with vs. w/o serrations) in the 1/3-octave band with a center frequency f_m = 1 kHz for a wide range of serration flap angles is plotted in the upper diagram of Fig. 9. Clearly, maximum noise reduction is achieved for fixed serration flap angles between ϕ = 10° and 15°. The self-aligning flap angle is lower than the optimum angle and provides smaller but still substantial noise reduction. The lower diagrams in Fig. 9 illustrate the effect of the airfoil angle of attack α_{eff} = 2.5°, 3.5° and 4.5° - here in case of serrations type *S II*. The self-aligning serration flap angles become smaller as the airfoil angle of attack is increased, and again: Noise reduction is existent but not maximum as for fixed flap angles.

Fig. 10 contains data for the case when the serrations are allowed to self-align in the flow. It is worth to note that in all experiments the self-aligning serrations stayed absolutely stable in the airfoil wake, no flow induced oscillations perpendicular to the mean flow were observed. Thus the self-aligning flap angle ϕ_{sa} measured is rather accurate. The torque to turn the serration out of their self-alignment position is remarkably large. The red dotted arrows in Fig. 9 indicate the data points ϕ_{sa} for self-aligning serrations. Irrespective of α_{eff} , the noise reduction is always approximately 5 dB in the 1 kHz frequency band. Clearly, ϕ_{sa} is acoustically not absolutely optimal but already shows a substantial noise reduction. And ϕ_{sa} varies with α_{eff} in the same sense as the optimal flap angles. Not shown here, the same tendencies are observed in other frequency bands up to the cross-over frequency. Hence, the initial first hypothesis that self-aligning serrations are superior when the airfoil angle of attack is varying (e.g. due to gusts of pitch control) can partly be confirmed. More noise reduction is possible with steeper than self-aligning flap angles of the serration, fixed for each α_{eff}. This points to the second initial hypothesis, that self-aligning serrations produce a noise reduction without increase of blade load, i.e. the flow induced forces on the blade. Fig. 11 shows the measured streamwise static pressure distribution for

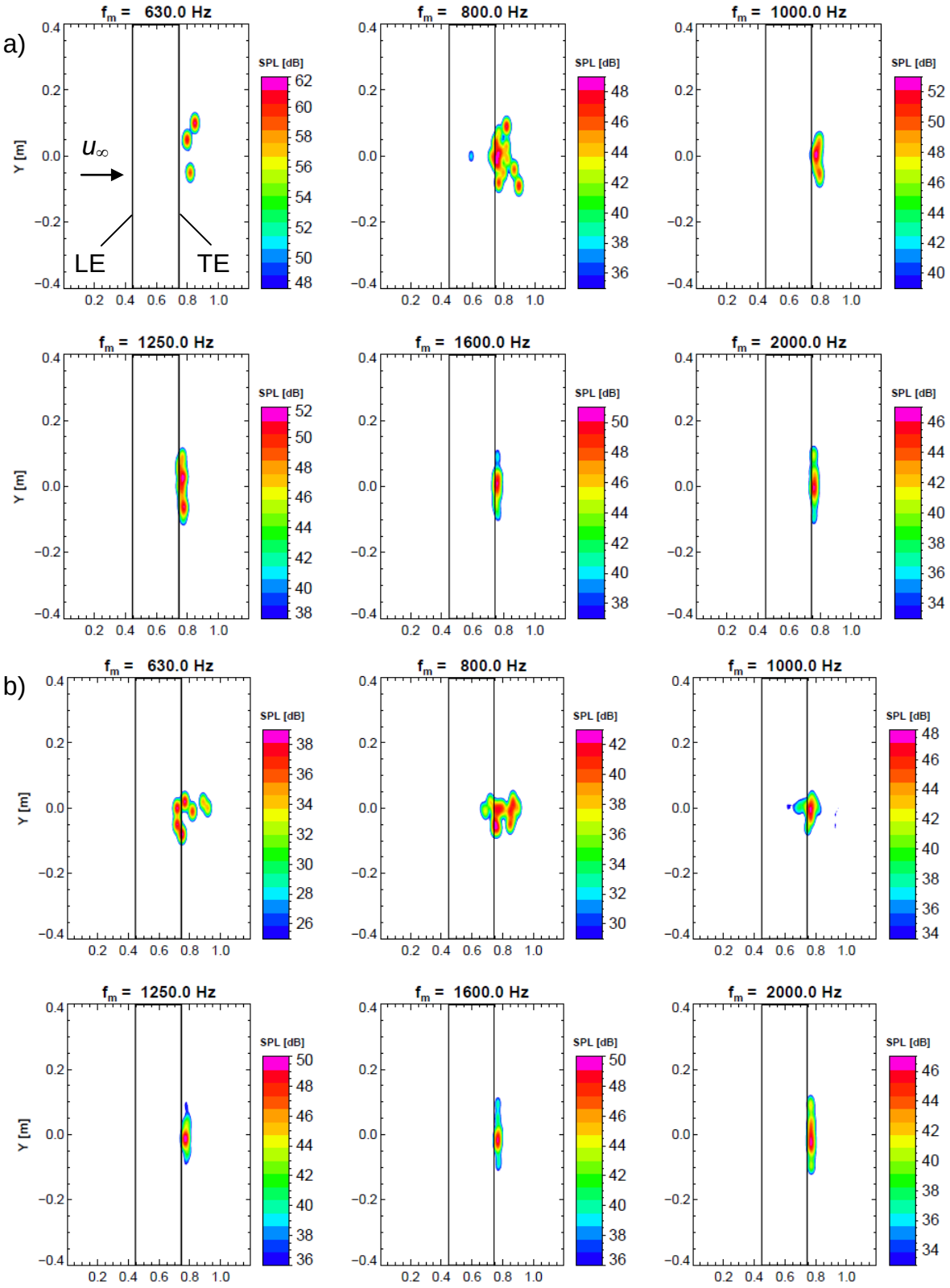

Figure 7: 1/3-octave band sound source map measured with the microphone array at α_{eff} = 3.5°, a) without serrations, b) with serrations S *I* at a fixed flap angle ϕ = 9.6°.

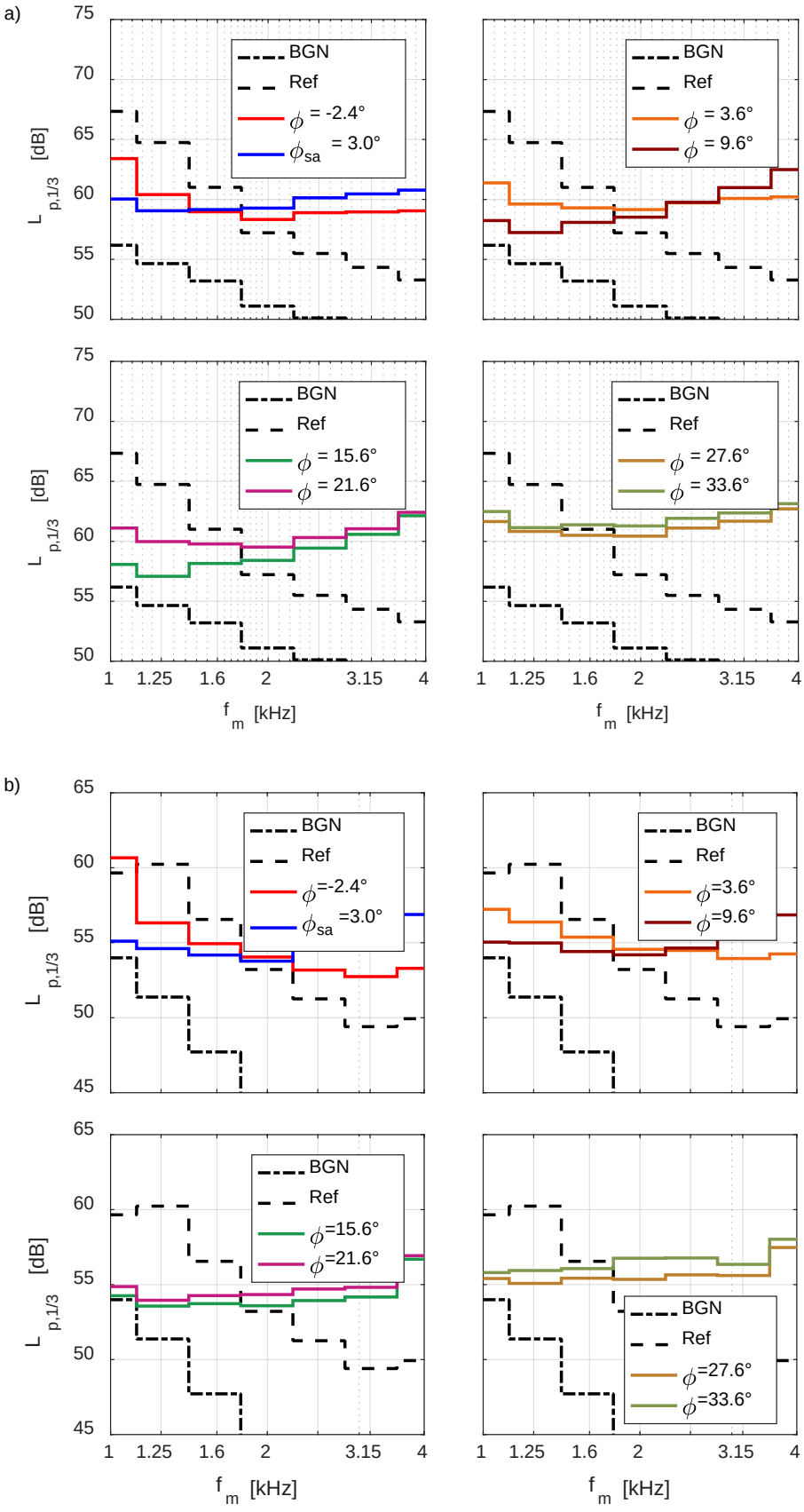

Figure 8: Far field 1/3-octave noise spectra for various fixed and self-aligning (sa) flap angles ϕ and α_{eff} = 3.5°, serrations S *1* a) from mirror, b) from microphone array.

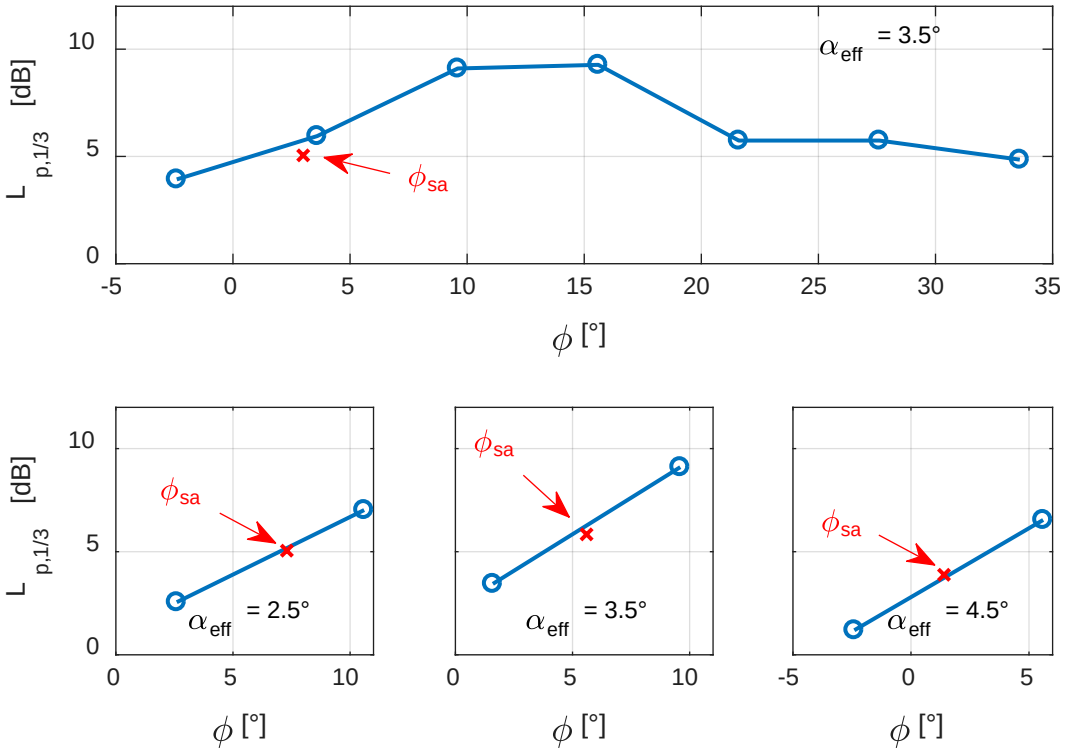

Figure 9: Noise reduction $\Delta L_{p,1/3}$ (with vs. w/o serrations) in the 1/3-octave band with a center frequency f_m = 1 kHz; upper: as a function of serration flap angle ϕ (serrations S *I,* taken from Fig. 8*)*; lower: as a function of airfoil angle of attack α_{eff} (S *II*, taken from Fig. 10*)*; the red crosses indicate the self-aligning flap angle, i.e. self-alignment of the serrations is permitted.

fixed and self-aligning serrations at α_{eff} = 3.5° and the reference without serrations. Note that *x*/*c* = 1 indicates the TE of the airfoil without serrations. For all practical reasons the pressure distribution is not affected by the serrations. Hence, fixed serrations as an add-on to a blade result in an increase of the flow induced force on the blade just due to the net increase of blade area - for the serrations tested here by appr. 8%. Self-alignment of the serrations will prevent this.

4. Summary and Conclusions

Two selected serrations were attached to a two-dimensional DU93W210 airfoil segment and tested at a Reynolds number of 1.2 mio. The experiment was carried out in two steps. Firstly, different *fixed* flap angles had been tested in order to find the acoustically most efficient flap angle. Secondly, *self-alignment* of the serrations was allowed, while the airfoil angle of attack was varied. The initial hypothesis that self-aligning serrations are superior when the airfoil angle of attack is varying (e.g. due to gusts of pitch control) can partly be confirmed. More noise reduction is possible with steeper than self-aligning flap angles of the serration, adapted to each airfoil angle of attack α_{eff}. Then the serrations need to be fixed. Fixed serrations as an add-onto a blade, however, result in an increase of the flow induced force on the blade just due to the net increase of blade area - the streamwise pressure distribution is not affected by the existence of serration. A work around is the integration in the initial blade design - not considered here.

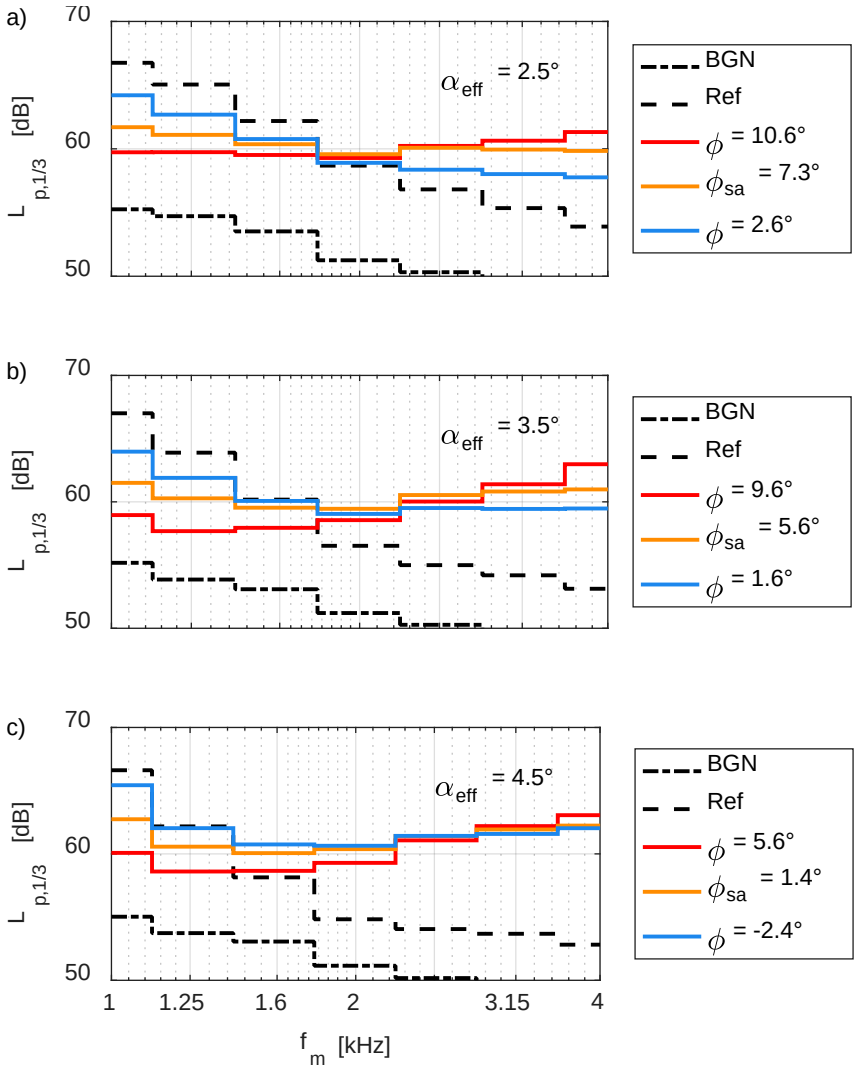

Figure 10: Far field 1/3-octave noise spectra: Self-adjusting serrations compared to fixed flap angles and the reference for different angles of attack (S *II)*.

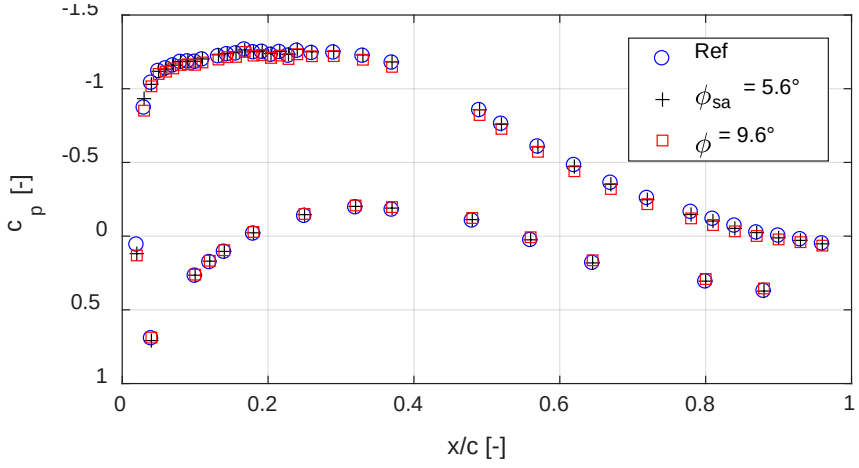

Figure 11: Streamwise static pressure distribution for fixed and self-aligning serrations (α_{eff} = 3.5°). "Ref" is the airfoil section without serrations. *x/c* = 1 indicates the TE of the airfoil without serrations.

5. Acknowledgement

Financial support for this work was partly provided by the Federal Ministry for Economic Affairs and Energy of Germany (BMWi) within the project RENEW (FKZ 0325838B). We also would like to thank B. Homrighausen and E. Bender from the University of Siegen for the design and manufacture of the instrumented model and for their support during the experimental phase in the wind tunnel. Finally we would like to thank the DLR Team in Braunschweig, especially M. Herr and K. Rossignol for the help and support during our measurement campaign.

6. References

[1] WAGNER, S., BAREISS, R., GUIDATI, G., *"Wind Turbine Noise"*, Springer, 1996.

[2] OERLEMANS, S., FISHER, M., MAEDER, T. AND KÖGLER, K., *"Reduction of Wind Turbine Noise using Optimized Airfoils and Trailing-Edge Serrations"*, 14th AIAA/CEAS Aeroacoustics Conference, Vancouver, Britisch Columbia Canada, 2008.

[3] OERLEMANS, S., SIJTSMA, P. AND MÉNDEZ LÓPEZ, B., "*Location and quantification of noise sources on a wind turbine"*, Jounal of Sound and Vibration, Volume 299, Issues 4-5, 2007.

[4] ARCE, C., RAGNI, D., PRÖBSTING, SE., SCARANO, F., *"Flow Field Around a Serrated Trailing Edge at Incidence"*, AIAA SciTech, 33rd Eind Energy Symposium, Kissimmee, Florida, 2015.

[5] ARCE, C., MERINO-MARTINEZ, R., RGNI, D., PRÖBSTING, S., AVALLONE, F., SINGH, A. AND MADSEN, J., *"Trailing Edge Serrations — Effect of Their Flap Angle on Flow and Acoustics"*, 7th International Conference on Wind Turbine Noise, Rotterdam, 2017.

[6] TIMMER,W.A., VAN ROOIJ,R.P.J.O.M., *"Summary of the Delft University Wind Turbine Dedicated Airfoils"*, 41st Aerospace Sciences Meeting and Exhibit, Reno, Nevada, 2003.

[7] GRUBER, M., JOSEPH, P.F., CHONG, T.P., *"On the mechanisms of serrated airfoil trailing edge noise reduction",* 17th AIAA/CEAS Aeroacoustics Conference, Portland, Oregon, 2011.

[8] POTT-POLLENSKE, M. and DELFS, J., *"Enhanced Capabilities of the Aeroacoustic Wind Tunnel Braunschweig"*, 14th AIAA/CEAS Aeroacoustics Conference, Vancouver, British Columbia, Canada, 5-7 May 2008, AIAA Paper 2008-2910, 2008.

[9] HERR, M., "*Trailing-Edge Noise*", Dr.-Ing. Dissertation, Technische Universität Carolo-Wilhelmina zu Braunschweig, 2013.

[10] ROSSIGNOL, K. S., HERR, M., SURYADI, A., *"Senvion AWB Studie Part 2: Acoustic measurements at a wind tunnel model in AWB, in cooperation with Universität Siegen",* Technical Report, Deutsches Zentrum für Luft und Raumfahrt e.V., Braunschweig, 2018.

[11] DOBRZYNSKI, W.; NAGAKURA, K., GEHLHAR, B. AND BUSCHBAUM, A., *"Airframe Noise Studies on Wings with Deployed High-Lift Devices"*, 4th AIAA/CEAS Aeroacoustics Conference, Toulouse, France, June 2-4 1998, AIAA Paper 98-2337, 1998.

[12] SIJTSMA, P., *"CLEAN based on spatial coherence"*, International Journal of Aeroacoustics", Vol. 6, No. 4, pp. 357-374, 2007.

[13] DRELA, M., YOUNGGREN, H., *"XFOIL 6.94 User Guide"*, Technical Report, Massachusetts Institute of Technology, Cambridge, 2001.